Aerial Drone Magnetometry for the Detection of Subsurface Unexploded Ordnance (UXO) in the San Gregorio Experimental Site (Zaragoza, Spain)

Ignacio Ugarte-Goicuría , Diego Guerrero-Sevilla , Pedro Carrasco-Garcia , Javier Carrasco-Garcia , Diego González-Aguilera *

Posted Date: 4 December 2025

doi: 10.20944/preprints202512.0511.v1

Keywords: aerial drones; aerial drone magnetometry; unexploded ordnance (UXO) detection; CENAD San Gregorio; geophysical surveying; ferromagnetic noise

Article

Aerial Drone Magnetometry for the Detection of Subsurface Unexploded Ordnance (UXO) in the San Gregorio Experimental Site (Zaragoza, Spain)

Ignacio Ugarte-Goicuría [1], Diego Guerrero-Sevilla [2] Pedro Carrasco-Garcia [2], Javier Carrasco-Garcia [2] and Diego Gonzalez-Aguilera [2,*]

[1] University Defense Center, General Military Academy

[2] Cartographic and Land Engineering Department, Higher Polytechnic School of Avila, Universidad de Salamanca, 37008 Salamanca, Spain

* Correspondence: daguilera@usal.es

Highlights

What are the main findings?

- Drone aerial magnetometry reliably detects small unexploded ordnance (UXO) (2–18 nT) at an altitude of 2 m, despite severe ferromagnetic noise (SNR > 5) in active controlled outdoor testing/training areas.
- A geolocation accuracy of approximately ~0.5 m was achieved, enabling precise planning of ground interventions.

What are the implications of the main findings?

- The method provides a safer alternative and is up to ten times faster than manual ground-based techniques, surveying 0.53 ha in less than one hour of effective flight time.
- The technology is scalable for integration into routine post-exercise inspection protocols and the management of contaminated areas in European military training centers.

Abstract

Unexploded ordnance (UXO) poses a significant hazard in controlled outdoor testing/training areas. This paper assesses the effectiveness of aerial drone-mounted magnetometry for detecting buried UXO located outside the designated designated landing areas of the National Training Center (CENAD) of San Gregorio (Zaragoza, Spain), considered the largest maneuver area in Europe. To this end, a high-resolution aeromagnetic survey was conducted using a GEM GSMP-35U proton magnetometer mounted on a hexacopter drone. Data were collected at flight altitudes of 7 m and 2 m above ground level along a grid with 1-m line spacing. For its validation, eleven UXOs were deliberately buried at known coordinates to evaluate the system's sensitivity and spatial resolution under operational conditions. The results demonstrate the capability of aerial drone-based magnetometry to detect small magnetic anomalies (with amplitudes between 2 and 18 nT) associated with buried UXO in complex environments characterised by high ferromagnetic noise, achieving signal-to-noise ratios greater than 5 (SNR > 5) at 2-m altitude and a geolocation accuracy of approximately 0.5 m. These findings support the use of unmanned aerial magnetometry as a viable tool for identifying hazardous remnants in military training ranges and field scenarios, enabling coverage of 0.53 ha in less than one hour of effective flight time.

Keywords: aerial drones; aerial drone magnetometry; unexploded ordnance (UXO) detection; CENAD San Gregorio; geophysical surveying; ferromagnetic noise

1. Introduction

Unexploded ordnance (UXO) remains a persistent hazard in controlled outdoor testing/training areas worldwide, posing risks to personnel safety, limiting land use, and generating long-term

 doi:10.20944/preprints202512.0511.v1

environmental impacts. In the Spanish Army's National Training Centers (CENAD), where controlled high-energy discharge exercises with heavy large-caliber devices are routinely conducted, a non-negligible proportion of metallic cylindrical objects either fail to detonate or land outside designated designated landing areas due to ballistic deviations, weapon-system malfunction, or adverse meteorological conditions. The detection and clearance of UXO in these environments is therefore a critical operational requirement.

Historically, UXO localisation has relied primarily on ground-based methods, including handheld or cart-mounted magnetometry and electromagnetic induction (EMI) systems [1–3]. Although these techniques offer high spatial resolution, they involve substantial logistical effort, expose personnel to hazardous terrain, and become inefficient or impractical in areas with dense vegetation, complex topography, or extensive ferromagnetic debris. These limitations have driven the development of aerial drones equipped with high-sensitivity magnetometers, which provide an appealing combination of spatial resolution, broad aerial coverage, and improved operator safety. Recent advances in sensor miniaturisation, flight control stability, and multirotor autonomy have enabled high-density aeromagnetic surveying at very low altitudes over complex and potentially dangerous terrain [4–6]. Aerial drones-based magnetic surveys are particularly advantageous in environments characterised by intense superficial ferromagnetic contamination—such as shrapnel, cartridge casings, and target fragments—where precise discrimination between background noise and anomalies associated with buried UXOs is essential [7–9].

1.1. Brief State of the Art

1.1.1. Magnetic Detection Principles

Magnetometry detects perturbations in the ambient geomagnetic field generated by ferromagnetic bodies whose magnetic susceptibility contrasts sharply with surrounding materials. Foundational geophysical texts [8,10] describe how artillery shells and similar UXO types produce dipolar anomalies whose amplitude decreases with the cube of the distance between sensor and target, imposing stringent requirements on sensor sensitivity and survey altitude. Modern overviews of magnetic methods [11] highlight the continuous evolution from 19th-century magnetic balances to contemporary high-precision proton-precession and optically pumped magnetometers, emphasising that UXO detection—given typical projectile diameters of 50–155 mm and shallow burial depths—requires sensitivities on the order of ≤0.01 nT and dense spatial sampling. These works also underscore the importance of correcting magnetic measurements for diurnal geomagnetic variations and anthropogenic noise, which are essential to enhancing SNR in UXO applications.

1.1.2. Conventional Ground and Airborne UXO Detection

Ground-based geophysical techniques—magnetometry, EMI, and ground-penetrating radar (GPR)—remain standard in operational demining due to their proximity to the target and resulting high sensitivity. However, they are slow, labour-intensive, and potentially hazardous. Early helicopter-borne aeromagnetic surveys demonstrated the potential to rapidly delimit contaminated areas, though flight altitudes of 30–50 m significantly limited detection of small UXO [3,12]. These pioneering studies established key principles: (i) helicopter magnetometry is effective for regional reconnaissance; (ii) detection of small-caliber UXO requires sensor–target distances of only a few meters; and (iii) integrating complementary methods (e.g., magnetometry and GPR) improves depth estimation and target characterisation [9].

These insights motivated the exploration of low-altitude, high-resolution unmanned systems as an intermediate solution between broad-scale airborne reconnaissance and fine-scale ground surveys.

 doi:10.20944/preprints202512.0511.v1

1.1.3. Aerial Drone Platforms for High-Resolution Magnetometry

The integration of high-sensitivity magnetometers with aerial multirotor drones has substantially expanded the capability of magnetic surveying. Aerial drones provide unique operational advantages: hovering capability, low-speed flight (1–10 m/s), heights of 1–10 m above ground level, and centimeter-level trajectory control via precise Global Navigation Satellite System (GNSS) and inertial measurement units (IMUs).

However, aerial drone-based magnetometry presents challenges absent in manned aircraft. Attitude variations (pitch, roll, yaw) can introduce orientation-dependent errors—particularly in optically pumped magnetometers—and magnetic interference from onboard ferromagnetic components can generate perturbations of 10–50 nT at short distances [13]. Best-practice guidelines established by Walter et al. [4,14] include: (i) suspending the magnetometer ≥2 m below the aerial drone on a nonmagnetic arm; (ii) characterising the aerial drone's magnetic signature; (iii) applying IMU-based attitude corrections; and (iv) conducting surveys under moderate wind and controlled speeds. These measures are now widely adopted as standard protocol [15].

1.1.4. Applications of Aerial Drone Magnetometry to UXO Detection

In the last decade, aerial drone-mounted magnetometry has been increasingly tested in post-conflict areas and active large-scale outdoor ranges [5,16–18]. One of the most rigorous studies to date was conducted in the Korean Demilitarised Zone (DMZ) [6], where a DJI Matrice 600 Pro carrying a GEM GSMP-35U proton magnetometer (the same sensor used in the present study) surveyed calibrated UXO test fields. Systematic tests at 2, 5, and 10 m above ground level demonstrated the cube-law attenuation predicted by magnetic theory [11]: 100% detection at 2 m, 85% at 5 m, and only 45% at 10 m, with corresponding decreases in anomaly amplitude and increases in positional error. The results established ≤3 m above ground level as the operational threshold for reliable detection of medium-caliber UXO (<120 mm), influencing subsequent international demining protocols.

Hybrid systems combining UAV magnetometry with terrestrial time-domain electromagnetic (TEM) surveys have also proven effective [5]. While aerial drone magnetometry rapidly highlights ferromagnetic anomalies, TEM data allow discrimination between UXO and scrap metal based on their characteristic electromagnetic decay properties. This combined approach reduced false positives from 43% to 25% in controlled tests, substantially lowering excavation costs and operational burden.

1.1.5. Sensor Technologies for Aerial Drone Magnetometry

Comparative studies of magnetometer technologies—proton precession, optically pumped alkali-vapour, and fluxgate sensors—have clarified their relative strengths and limitations for aerial drone deployment [15]. Proton magnetometers offer high absolute sensitivity and orientation-independence at moderate cost, making them suitable for UXO detection at ≤1 m depth. Optically pumped cesium systems support high sampling rates and are advantageous for high-speed surveys, but are costlier and orientation-sensitive. Fluxgate magnetometers, while inexpensive and robust, lack the sensitivity required for detecting small UXOs at more than minimal heights. Experimental comparisons confirm that proton and cesium sensors detect nearly all UXOs at ≤3 m above ground level, whereas fluxgate systems perform poorly above ~2 m.

1.1.6. Advances in Magnetic Data Processing

Quantitative interpretation of magnetic anomalies requires advanced processing techniques, notably 3D magnetic inversion. Li and Oldenburg [19,20] introduced algorithms that remain the methodological standard for estimating subsurface susceptibility distributions and target depth. Although challenges persist—such as anomaly superposition and noise introduced by dense ferromagnetic debris—these inversion methods can estimate UXO depth with ±15–20% error, sufficiently accurate to guide excavation priorities [21].

 doi:10.20944/preprints202512.0511.v1

1.2. Research Gaps and Study Motivation

Despite recent advances highlighted above, several critical gaps persist in the literature: (i) Lack of data from active large-scale outdoor ranges with realistic ferromagnetic contamination. Most published test sites have relatively clean magnetic backgrounds compared with modern active ranges, where dense shrapnel and metal debris generate RMS noise >10 nT, complicating UXO detection [22–24]. (ii) Limited systematic assessment of flight altitude under complex topographic and environmental conditions. Existing studies rarely evaluate low-altitude (≤2 m) versus moderate-altitude (5–7 m) operation in irregular terrain or dense metal clutter. (iii) Insufficient ground-truth validation. Few works report fully quantified performance metrics (detection rate, false positives, geolocation accuracy) for UXO buried at surveyed, geodetically verified coordinates [25]. (iv) Absence of documented applications in European geomagnetic and regulatory contexts. Differences in geomagnetic inclination (60–65°), European Union UAV regulations, and standardized large-caliber metallic objects necessitate region-specific validation. (v) Lack of end-to-end operational workflows. Most studies focus on isolated components (sensor technology, algorithms) rather than integrated methodologies ready for routine military use [26].

Therefore, the present work addresses these gaps by evaluating the effectiveness of aerial drone-mounted magnetometry for detecting UXOs in one of Europe's largest active controlled outdoor testing/training area: the CENAD San Gregorio (Zaragoza, Spain). Using a high-sensitivity GEM GSMP-35U proton magnetometer mounted on a hexacopter and flown at very low altitudes (2–7 m), we conducted a high-resolution aeromagnetic survey over terrain characterised by complex topography and intense ferromagnetic contamination.

In this study, particular emphasis is placed on the technical methodology and data-processing required to reliably detect weak magnetic anomalies in high-noise environments. The workflow integrates diurnal correction, noise filtering, spectral transformations (Reduction to the Pole, analytic signal), and 3-D magnetic susceptibility inversion. These steps constitute a technical contribution of the work and are essential for enhancing anomaly detectability, improving positional accuracy, and enabling quantitative interpretation of buried ferromagnetic targets.

2. Materials and Methods

2.1. Study Area

The field experiment was conducted at the San Gregorio National Training Center (Centro de Adiestramiento de San Gregorio, CENAD), located near Zaragoza, Spain (Figure 1a). The training area covers approximately 33,000 ha (340 km²) and is considered the largest manoeuvre range in Europe, with a perimeter of about 108 km (Figure 2). The selected test site is characterised by gently undulating topography, sparse steppe-type vegetation (Figure 1b), and a high density of metallic debris associated with controlled high-energy discharge exercises, providing an ideal setting to evaluate aeromagnetic survey techniques in a complex, noise-contaminated environment [27].

 doi:10.20944/preprints202512.0511.v1

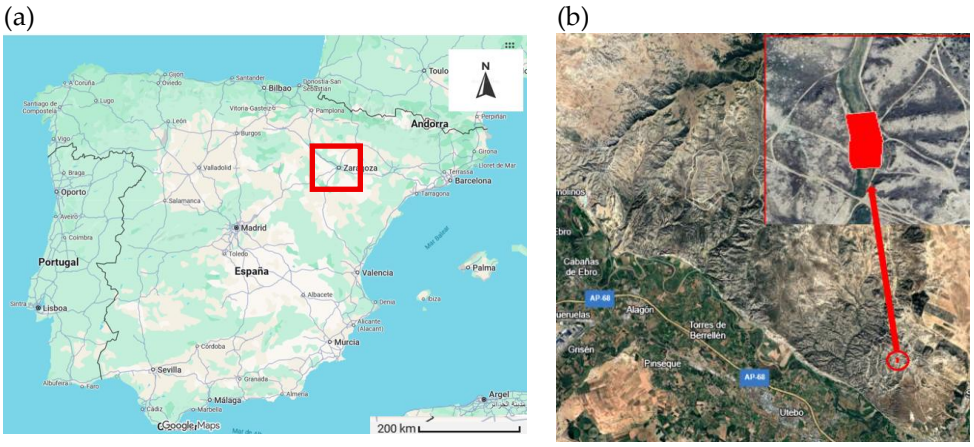

Figure 1. (a) Map of Spain showing the location of Zaragoza, obtained from Google Maps. (b) Orthophoto of the San Gregorio CENAD showing the specific test area located on the perimeter firebreak of the F-23 projectile designated landing area.

The regional location of Zaragoza within Spain, the official 1:50,000 topographic map of the CENAD, and an orthophoto showing the specific test area along the perimeter firebreak of the F-23 projectile designated landing area are presented in a composite figure (Figure 2).

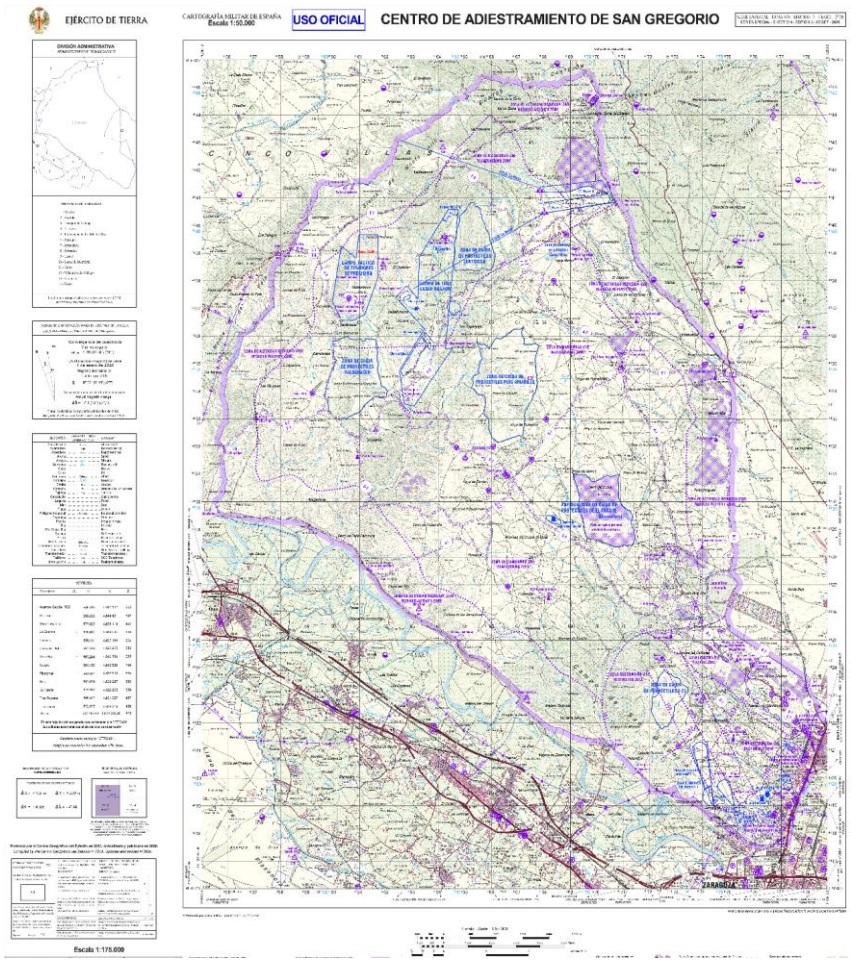

Figure 2. Official map of the San Gregorio CENAD at a 1:50,000 scale.

The particular sector chosen for the experimental survey exhibits low direct anthropogenic interference, limited ground accessibility via unpaved tracks, and a moderate density of superficial

 doi:10.20944/preprints202512.0511.v1

ferromagnetic elements, making it suitable for validating aerial drone-based aeromagnetic methods under realistic field conditions (Figure 1b).

2.2. Experimental Design

To assess the detection capability of the aerial drone–magnetometer system, a set of 11 unexploded ordnance (UXO) surrogates of different diameters and morphologies (60, 81, 105, 120, and 155 mm) were deliberately buried at known positions within the study area. Burial depths ranged from 20 to 60 cm, reproducing realistic field conditions encountered in active military training ranges.

The main characteristics of the metallic cylindrical objects used in the experimental campaign—including caliber, burial depth, material, orientation, approximate mass, and ferrous content—are summarised in Table 1.

Table 1. Characteristics of the UXO surrogates buried for the experimental survey.

Type	Caliber (mm)	Burial Depth (cm)	Material	Orientation	Approx. Mass (kg)	Ferrous Content
Mortar shell	60	20–30	Ferromagnetic	Horizontal	2.5	Yes
Mortar shell	81	30–40	Ferromagnetic	Vertical	4.4	Yes
Artillery projectile	105	40–50	Ferromagnetic	Horizontal	15.7	Yes
Mortar shell	120	50–60	Ferromagnetic	Vertical	13.5	Yes
Artillery projectile	155	20–60	Ferromagnetic	Horizontal	43.2	Yes
Anti-tank projectile (C/C)	—	30	Plastic (non-ferrous)	Horizontal	4.5	No (negative control)

Note: The ferromagnetic metallic cylindrical objects were buried in known positions for system validation. The anti-tank projectile was included as a negative control to verify the absence of a magnetic response in non-ferrous objects. The masses are approximate and based on standard military ammunition specifications.

In addition to ferromagnetic munitions, an anti-tank projectile with a plastic (non-ferrous) body was included as a negative control to verify the absence of magnetic response from non-ferromagnetic objects. All ferromagnetic metallic cylindrical objects were buried at geodetically surveyed coordinates to enable quantitative validation of the detection results.

Representative photographs of the different metallic cylindrical objects and their emplacement in the field are presented as a mosaic in Figure 3a-f, including the full set of UXO surrogates, the 105 mm projectile and its placement, the 120 mm mortar shell in vertical orientation, the 155 mm projectile, the 60 mm mortar shell, and the negative-control anti-tank projectile during installation.

 doi:10.20944/preprints202512.0511.v1

(a)

(b)

(c)

(d)

(e)

(f)

 doi:10.20944/preprints202512.0511.v1

Figure 3. (a) Set of metallic cylindrical objects used in the experimental campaign to simulate buried UXO. (b)105 mm projectile and detail of its placement in the ground during the test. (c) 20 mm mortar round placed in a vertical position for data collection. (d)155 mm projectile and detail of its placement in the ground. (e) 60 mm mortar round and detail of its placement in the ground. (f) Details of the placement process for the negative-control anti-tank projectile.

The UXO surrogates were distributed in a dispersed pattern over an area of 0.53 ha, aligned with the existing perimeter firebreak. This layout facilitated the design of flight lines and maximised effective magnetic coverage while maintaining operational safety for the UAV platform.

2.3. Acquisition Platform

The aeromagnetic survey was carried out using a multirotor hexacopter aerial drone programmed for autonomous flights based on a digital terrain model (DTM) of the study area. The main sensor was a GEM GSMP-35U proton-precession magnetometer, mounted on a non-magnetic arm suspended beneath the aerial drone to minimise magnetic interference from the airframe, motors, and onboard electronics. A composite figure illustrating the installation of the GSMP-35U sensor beneath the hexacopter and its configuration for aeromagnetic surveying is included as part of the general methods (Figure 4).

 doi:10.20944/preprints202512.0511.v1

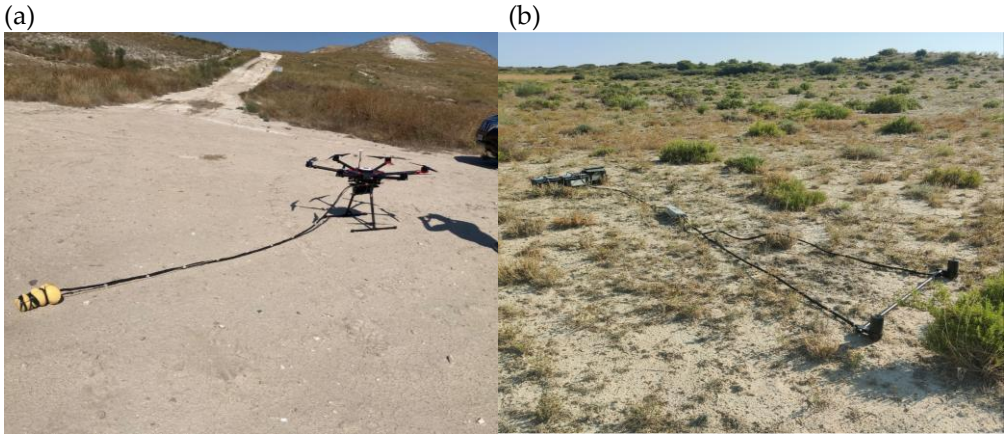

Figure 4. Field installation of the two magnetometer systems used in this study. (a) GEM GSMP-35U airborne magnetometer deployed in a towed-bird configuration beneath the hexacopter UAV for aeromagnetic surveying. (b) GEM GSMP-40 ground magnetometer arranged in a horizontal configuration for base-station and ground-reference magnetic measurements.

The key technical specifications of the hexacopter platform, the GEM GSMP-35U and GEM GSMP-40 magnetometers are summarised in Table 2.

Table 2. Technical specifications of the hexacopter aerial drone, the GEM GSMP-35U airborne magnetometer, and the GEM GSMP-40 base-station magnetometer.

Component	Parameter	Specification
Hexacopter aerial drone	Flight time	Up to 40 min (with 2 kg payload)
	Maximum payload	5 kg
	Operational range	20 km
	Wind resistance	Up to 32 km/h
	Airframe material	Carbon-fiber structure
	Navigation system	GPS/GNSS + barometric altimeter + electronic compass
GEM GSMP-35U Magnetometer	Sensor type	Potassium optically pumped magnetometer
	Sensitivity	0.0002 nT @ 1 Hz
	Resolution	0.0001 nT
	Dynamic range	20,000–120,000 nT (optional: up to 350,000 nT)
	Sampling frequency	1, 5, 10, or 20 Hz (max. 20 Hz)
	Sensor head dimensions	161 mm × 64 mm; weight: 0.43 kg
	Electronics module dimensions	236 mm × 56 mm × 39 mm; weight: 0.46 kg
GEM GSMP-40 Magnetometer	Sensor type	Potassium optically pumped magnetometer
	Sensitivity	0.0002 nT @ 1 Hz
	Resolution	0.0001 nT
	Dynamic range	20,000–100,000 nT (optional: 10,000–350,000 nT)
	Sampling frequency	1, 5, 10, or 20 Hz
	Sensor head dimensions	141 mm × 64 mm; 1.5 kg
	Electronics module dimensions	310 mm × 75 mm × 90 mm; 1.6 kg
	Operating temperature range	−20 °C to +55 °C (optional down to −40 °C)

In brief, the aerial drone offers a maximum flight time of up to 40 minutes with a 2 kg payload, a maximum payload capacity of 5 kg, an operational range of approximately 20 km, and wind tolerance up to 32 km/h. The airframe is constructed from carbon-fiber components, and navigation is provided by an integrated GPS/GNSS, barometric altimeter, and electronic compass.

The GSMP-35U proton magnetometer operates over a dynamic range of 20,000–120,000 nT, with a nominal sensitivity of 0.0002 nT at 1 Hz and a resolution of 0.0001 nT. The sampling frequency is configurable between 0.1 and 10 Hz, and the sensor is specified to operate between −10 °C and +50

 doi:10.20944/preprints202512.0511.v1

°C. All specifications follow the manufacturer's documentation (GEM Systems Inc., Ontario, Canada). Both the airborne sensor and the reference instrument were calibrated before the data acquisition campaign.

A ground-based base station equipped with a GEM GSMP-40 potassium (optically pumped) magnetometer (sensitivity 0.0002 nT, resolution 0.0001 nT) was deployed in a magnetically quiet location outside the main impact area. This station continuously recorded temporal variations in the geomagnetic field during the aerial drone surveys, enabling subsequent correction of diurnal variations in the airborne magnetic data. The role and basic characteristics of the base station are also included in Table 2.

2.4. Flight Planning and Aeromagnetic Survey

Data acquisition was planned for stable meteorological conditions to minimise atmospheric interference. Two consecutive aeromagnetic surveys were designed to be performed over the same area at different flight heights (7 m and 2 m above ground level) to systematically evaluate the influence of sensor–target distance on the magnetic response of buried UXO surrogates and enable direct comparison of detection performance, signal-to-noise ratios, and anomaly morphology.

Both surveys were designed along a regular grid of parallel flight lines with 1 m spacing, oriented parallel to the perimeter firebreak delimiting the test area. This configuration was selected to maximise area coverage while ensuring sufficiently dense spatial sampling for detecting small-scale magnetic anomalies associated with UXO.

Flight planning incorporated a high-resolution DTM to generate terrain-following flight paths, maintaining constant heights of 7 m and 2 m above ground level. This approach is critical for ensuring consistent sensor–target distances in undulating terrain and for minimising collision risk. The planned flight speed was 5 m/s with magnetometer sampling configured at 20 Hz, yielding a theoretical along-track spacing of approximately 0.25 m between successive measurements.

The survey design covered 0.53 ha (5,300 m²) in the F-23 perimeter firebreak sector using 42 parallel flight lines (total trajectory length ~21 km). All positional data were configured to be recorded in the WGS84/UTM zone 30N reference system to ensure accurate georeferencing for subsequent ground-truthing operations.

The planned sampling density (~0.25 m along-line × 1 m cross-line spacing) was selected as appropriate for resolving decametric-scale anomalies associated with metallic cylindrical objects in the 60–155 mm caliber range [4, 8].

The main technical parameters of the aeromagnetic surveys are compiled in Table 3.

Table 3. Technical parameters of the aeromagnetic survey conducted at the CENAD San Gregorio.

Parameter	Value	Remarks
Surveyed area	0.53 ha (5,300 m²)	Perimeter firebreak sector (F-23)
Flight-line spacing	1 m	Regular parallel grid
Total number of flight lines	42	Total trajectory length ~21 km
Flight speed	5 m/s	Constant for both campaigns
Sampling frequency	20 Hz	1 measurement every 50 ms (~25 cm spacing)
Flight heights	7 m and 2 m	Two independent consecutive surveys
Total measurements (7 m)	26,771 points	~50 points/ha
Total measurements (2 m)	26,771 points	~50 points/ha
Combined measurements	53,542 points	Both campaigns together
Acquisition date	14 July 2025	Stable meteorological conditions
Mean temperature	24 °C	Optimal for sensor stability
Wind speed	<10 km/h	Favourable for flight precision

 doi:10.20944/preprints202512.0511.v1

Parameter	Value	Remarks
Effective flight time	<1 hour	Includes both 7 m and 2 m surveys
Reference system	WGS84 / UTM zone 30N	Accurate georeferencing

Note: The sampling interval of ~25 cm between points enables the detection of magnetic anomalies at the hectometric to decametric scale, appropriate for metallic cylindrical objects ranging from 60 to 155 mm. The final geolocation accuracy (~0.5 m) results from the combined effect of the DTM error and the sampling spacing.

Figure 5 shows the flight plan designed for the study area considered. The total surveyed surface was 0.53 ha (5,300 m²) in the F-23 perimeter firebreak sector, covered by 42 parallel flight lines with 1 m spacing. The aerial drone maintained a constant ground speed of 5 m/s in both campaigns, with the magnetometer sampling at 20 Hz, corresponding to one measurement every 50 ms and an along-line spacing of approximately 0.25 m between successive points (Figure 5). The two flight heights (7 m and 2 m) resulted in identical numbers of recorded measurements (26,771 points per survey), for a combined total of 53,542 data points. Effective flight time for both surveys was less than one hour. All positional data were recorded in the WGS84/UTM zone 30N reference system.

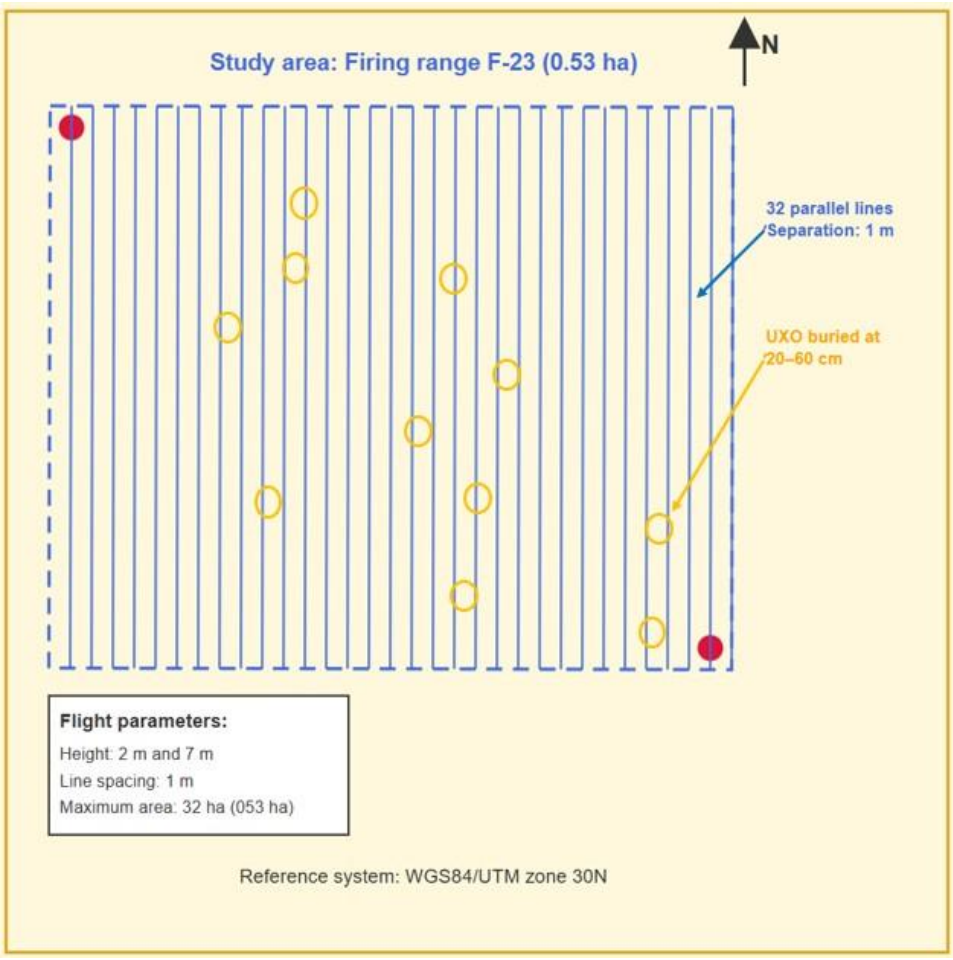

Figure 5. Flight plan designed for data acquisition.

The chosen sampling density (~0.25 m along-line spacing and 1 m line spacing) is appropriate for resolving decametric-scale anomalies associated with metallic cylindrical objects in the 60–155 mm caliber range. The stable meteorological conditions and low wind speeds during the survey contributed to flight stability and sensor performance, minimising attitude variations and platform-induced noise [4, 8].

 doi:10.20944/preprints202512.0511.v1

2.5. Rationale of the Acquisition Strategy

The acquisition parameters were selected to guarantee adequate spatial sampling for magnetic detection. The 20 Hz sampling rate combined with a 5 m/s flight speed produced an effective along-track spacing of ~0.25 m, sufficient to resolve short-wavelength anomalies generated by small ferromagnetic objects. The 1-m flight-line spacing ensured lateral oversampling, while the two flight altitudes (2 m and 7 m) allowed quantification of the cubic attenuation of magnetic amplitude ($1/r^3$). These acquisition choices were technically motivated to maximise the signal-to-noise ratio, minimise aliasing, and provide input data suitable.

2.6. Processing and Interpretation

The magnetic-data processing followed a structured workflow designed to enhance weak anomalies in cluttered environments. The processing sequence consists of six main stages:

1. Pre-processing and quality control: removal of spikes associated with take-off and landing, attitude-change artefacts, and platform-induced disturbances. These steps were performed using the Airborne Quality Control module in Oasis Montaj.
2. Diurnal correction: subtraction of the base-station time series to compensate for temporal geomagnetic variations.
3. Gridding: minimum-curvature interpolation using a cell size of 0.25–0.5 m, consistent with the acquisition spacing.
4. Noise filtering and signal enhancement: application of directional derivatives, high-pass and low-pass filters, and upward/downward continuation to suppress regional magnetic trends and emphasise short-wavelength responses associated with near-surface ferromagnetic sources. All these operations can optionally be performed within the Oasis Montaj environment, allowing users to visualise the results and familiarise themselves with the behaviour of the magnetic field.
5. Spectral transformations:

- Reduction to the Pole (RTP) to centre dipolar anomalies given the local inclination.
- Analytic Signal to obtain amplitude-only gradients independent of magnetisation direction and to highlight compact sources.

6. 3-D magnetic inversion: depth-constrained magnetic-susceptibility inversion performed using the VOXI Earth Modelling module in Oasis Montaj. The inversion enabling the estimation of subsurface susceptibility distributions and the derivation of the geometry and depth of the ferromagnetic sources. This 3-D modelling step provides a volumetric interpretation that complements the 2-D maps and enhances understanding of the spatial characteristics of the detected anomalies.

This processing chain represents the central methodological contribution of the study, enabling the identification of 2–18 nT anomalies despite intense ferromagnetic noise. Once the aerial drone magnetometry campaign was completed, the processing and interpretation workflow was applied in detail as described below (Figure 6).

 doi:10.20944/preprints202512.0511.v1

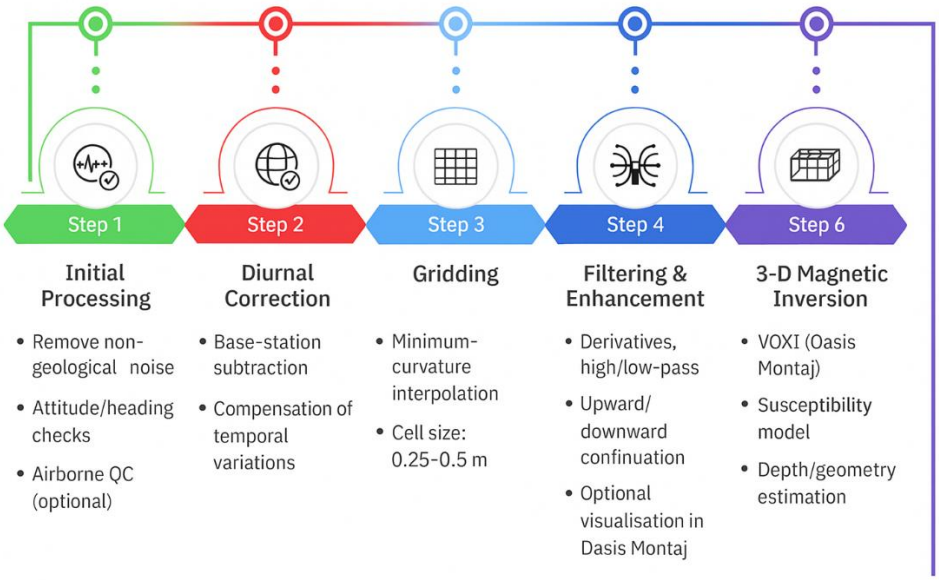

Figure 6. Processing and interpretation methodology developed for the detection of UXOs.

The raw magnetic data acquired by the aerial drone-mounted magnetometer underwent an initial quality-control and cleaning stage to ensure the integrity of the subsequent analysis (Figure 6, Step 1). Non-geological noise was first removed, including transient disturbances produced during take-off, landing, and platform manoeuvres such as sharp turns or velocity changes. These unstable segments were identified by examining the platform attitude logs and by detecting inconsistencies in the magnetic signal. Additional checks for heading errors, sensor saturation, and platform-induced disturbances were carried out using the Airborne Quality Control module in Oasis Montaj.

Diurnal magnetic variations were then corrected using data from a proximal base-station magnetometer (Figure 6, Step 2). The base-station time series was low-pass filtered and subtracted from the UAV data to compensate for temporal fluctuations in the Earth's magnetic field, significantly improving the signal-to-noise ratio.

Following these corrections, the magnetic data were interpolated into a regular 2-D grid using the minimum-curvature algorithm implemented in Oasis Montaj (Figure 6, Step 3). An optimised cell size between 0.25 and 0.5 m was selected according to the acquisition spacing and flying altitude, ensuring that short-wavelength magnetic features were preserved. From the resulting grid, total-field maps were generated.

To enhance the magnetic signature of potential ferromagnetic targets, a series of noise-filtering and signal-enhancement operations were applied (Figure 6, Step 4). These included directional derivatives, high-pass and low-pass filters, and upward/downward continuation to suppress regional magnetic trends while highlighting short-wavelength responses associated with shallow sources. All these operations can optionally be performed and visually inspected within Oasis Montaj, allowing the operator to familiarise themselves with the behaviour of the magnetic field.

Spectral transformations were then applied to improve anomaly interpretability (Figure 6, Step 5). Reduction to the Pole (RTP) was used to centre dipolar anomalies under the local geomagnetic inclination, while the Analytic Signal was computed to obtain amplitude-only gradients independent of magnetisation direction, effectively emphasising compact ferromagnetic bodies.

Finally, three-dimensional magnetic inversion was performed using the VOXI Earth Modelling platform in Oasis Montaj (Figure 6, Step 6). This depth-constrained inversion allowed the estimation of subsurface magnetic susceptibility and provided volumetric models that clarified the geometry

 doi:10.20944/preprints202512.0511.v1

and depth of the detected anomalies. The resulting 3-D susceptibility distribution complemented the 2-D maps and enhanced the spatial interpretation of the magnetic responses.

The final interpretation integrated all processed results with geological context and expert geophysical assessment. Magnetic anomalies were evaluated according to amplitude, dipole geometry, spatial coherence, and estimated depth. Anomalies consistent with compact ferromagnetic cylindrical bodies were identified as priority targets, while weaker or irregular responses likely related to cultural or geological noise were considered potential false positives. The resulting interpretation map provides a reliable, high-resolution framework for guiding ground-truthing and risk-assessment activities.

3. Experimental Results

The aeromagnetic survey conducted at the San Gregorio National Training Center (CENAD) clearly revealed the magnetic anomalies associated with the experimentally buried unexploded ordnance (UXO), even within an environment characterised by high levels of ferromagnetic background noise (diurnal variations up to ±3 nT) (Figure 7). The successive processing and interpretation stages are illustrated in the figures presented below, accompanied by an extended discussion to highlight their operational implications.

The application of the full processing workflow significantly improved the clarity of the magnetic anomalies. Diurnal correction reduced temporal noise, the RTP transformation recentred asymmetric dipoles under the local geomagnetic inclination, and the analytic signal isolated compact bodies associated with buried ferromagnetic targets. The combined effect of these processing steps yielded signal-to-noise ratios greater for all targets at the 2-m flight altitude.

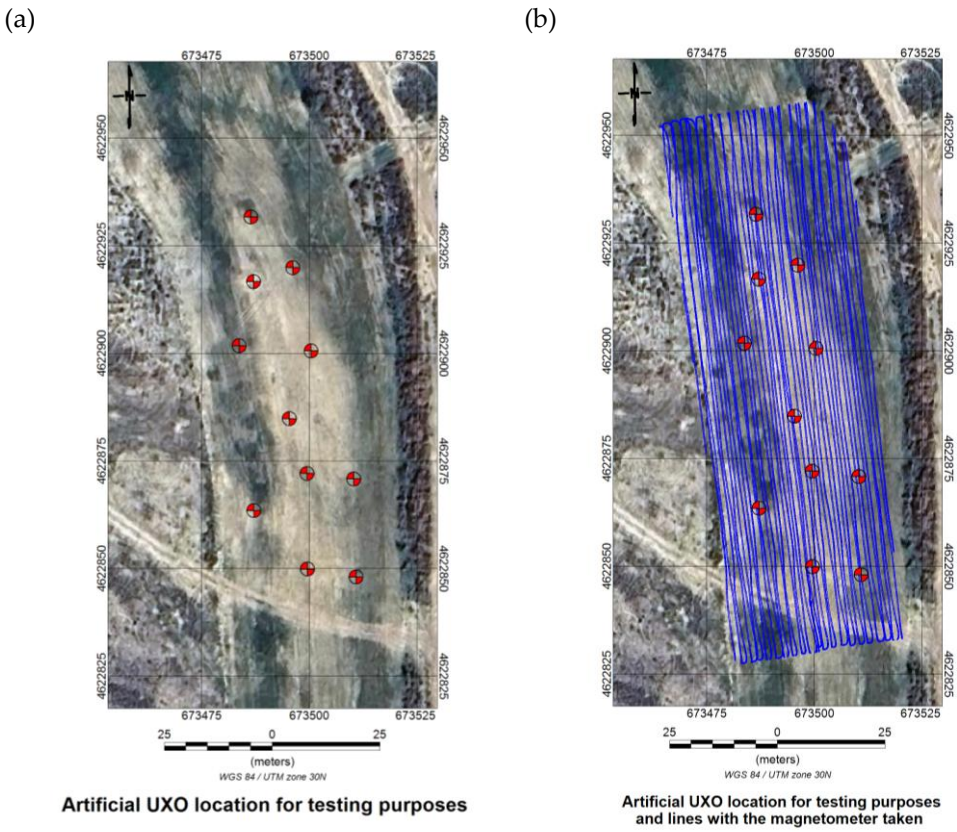

Figure 7. Spatial distribution of the buried UXO (a) and layout of the acquisition lines of the aeromagnetic survey (b). Reference system: WGS84/UTM zone 30N.

Figure 8 shows the comparison between the planned flight path and the actual flight trajectory executed.

 doi:10.20944/preprints202512.0511.v1

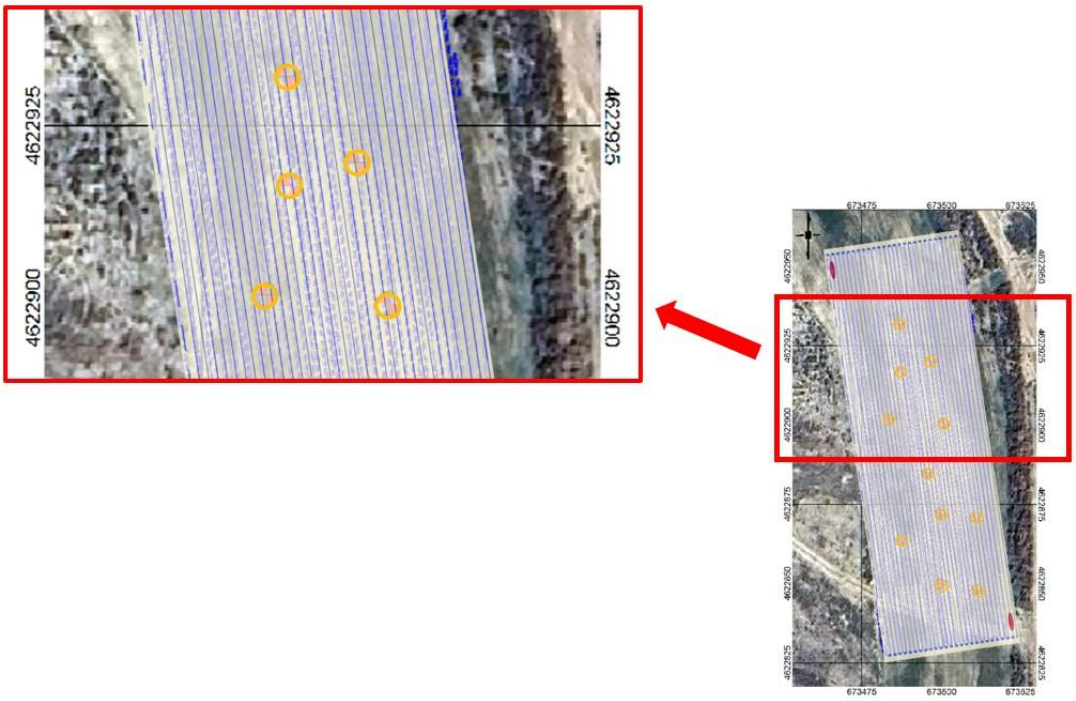

Figure 8. Superposition of the Planned Flight Path with the Executed Flight Trajectory. Reference system: WGS84/UTM zone 30N.

3.1. Survey Execution and Data Quality

The aeromagnetic survey was successfully executed on 14 July 2025 under favourable meteorological conditions, with a mean air temperature of 24 °C and wind speeds consistently below 10 km/h, conditions that proved optimal for sensor stability and flight precision. Both planned surveys (7 m and 2 m heights) were completed over the 0.53 ha test area, following the 42 parallel flight lines with 1 m spacing. The aerial drone maintained the programmed ground speed of 5 m/s throughout both campaigns, with the magnetometer sampling at the configured 20 Hz rate. This resulted in 26,771 georeferenced magnetic measurements per flight height, yielding a combined dataset of 53,542 data points (Figure 5). The effective total flight time for both surveys was less than one hour, demonstrating the operational efficiency of the aerial drone-based approach. The achieved sampling density of approximately 0.25 m along-track spacing and 1 m cross-track spacing provided coverage of ~50 measurement points per hectare, appropriate for detecting the 60–155 mm caliber metallic cylindrical objects buried in the test area.

Post-processing analysis confirmed a geolocation accuracy of approximately 0.5 m (RMSE), dominated by the combined effects of DTM uncertainty and the discrete sampling interval. The stable meteorological conditions during acquisition contributed to minimal attitude variations and reduced platform-induced magnetic noise, as evidenced in the base-station time series (Section 3.2).

The terrain-following capability enabled by DTM-based flight planning successfully maintained near-constant sensor heights above ground level despite local topographic variations, a critical factor for subsequent quantitative comparison of magnetic anomalies between the two flight campaigns

3.2. Diurnal Correction

The diurnal variation of the Earth's magnetic field, driven by ionospheric and solar phenomena, reached amplitudes of up to ±30 nT during data acquisition. Applying the diurnal correction using the potassium base-station magnetometer significantly stabilised the magnetic signal and improved the signal-to-noise ratio—particularly for the 7 m flight, where anomalies were inherently weaker due to the increased sensor–target distance. This correction step is essential in environments affected by temporal magnetic fluctuations, reducing background noise by approximately 30–50% and

 doi:10.20944/preprints202512.0511.v1

enabling the detection of subtle anomalies as low as 2 nT. Figure 9 shows the total magnetic field recorded during the 2 m flight (a) and the corrected magnetic field after applying the diurnal correction (b).

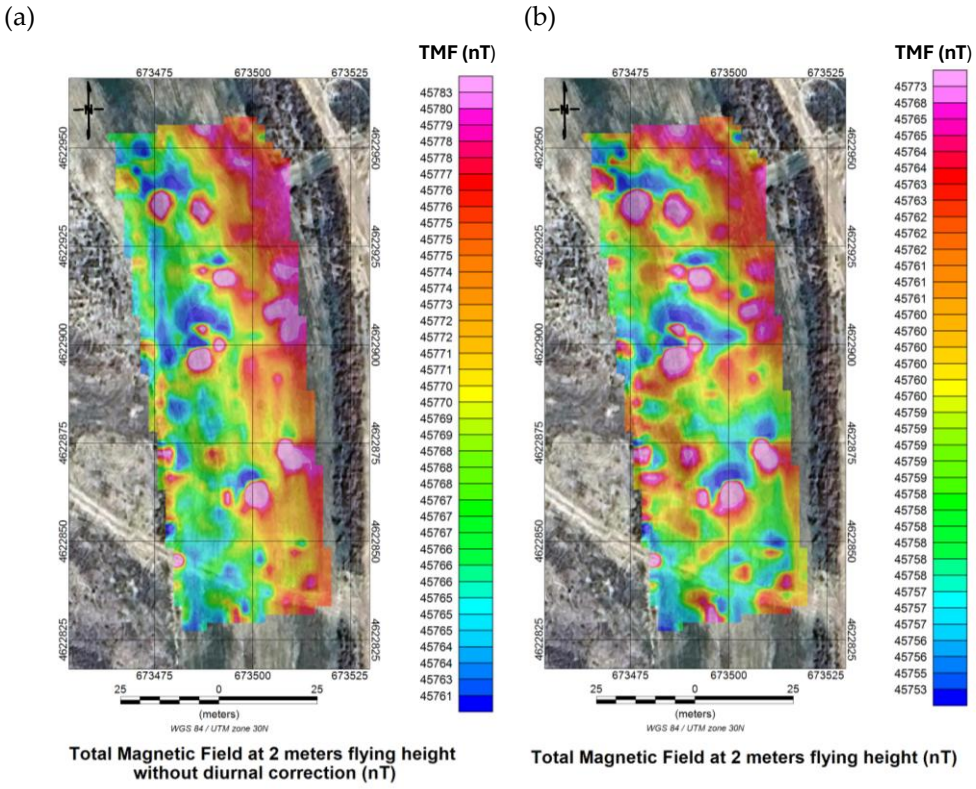

Figure 9. Total magnetic field recorded during the 2 m flight (a) and magnetic field corrected after applying the diurnal correction (b). WGS84/UTM zone 30N (scale in nT).

Figure 10 presents the same comparison for the 7 m flight. All maps are displayed in WGS84/UTM Zone 30N with magnetic field intensity in nT.

 doi:10.20944/preprints202512.0511.v1

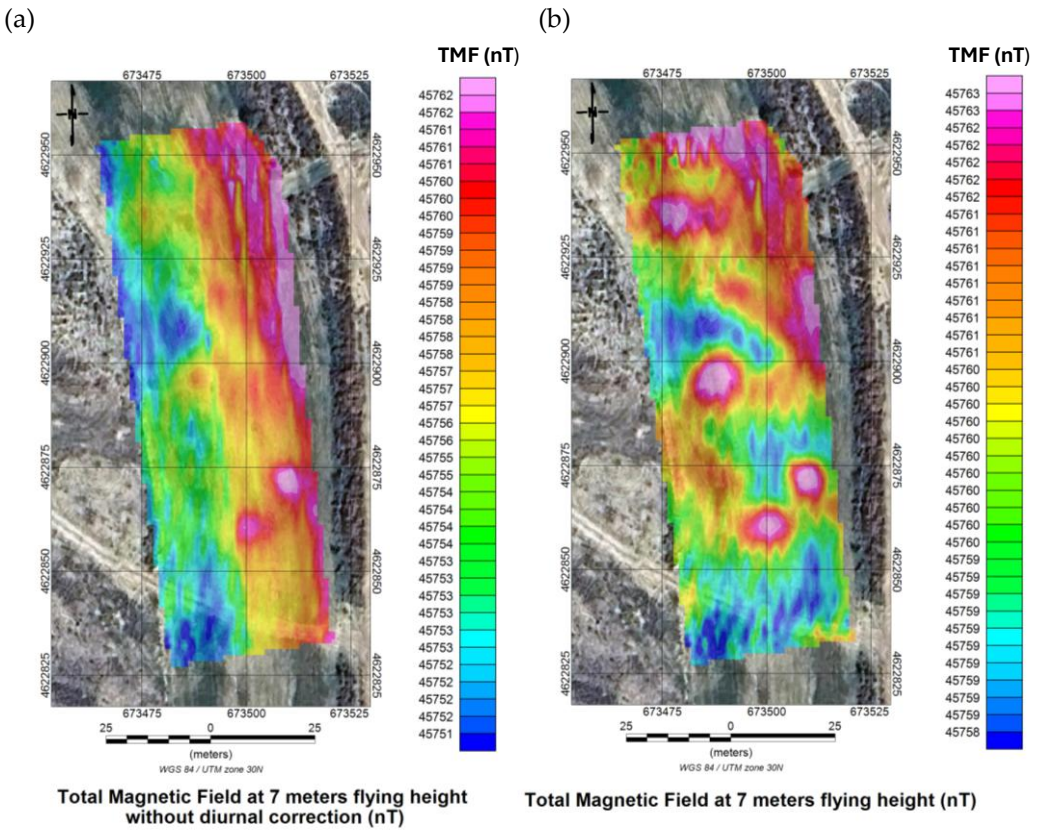

Figure 10. Total magnetic field recorded during the 7 m flight (a) and magnetic field corrected after applying the diurnal correction (b). WGS84/UTM zone 30N (scale in nT).

In both cases, a pronounced reduction in background noise is observed (from ±3 nT to <1 nT), together with enhanced definition of localised anomalies associated with the buried UXO. This improvement facilitates the identification of characteristic dipolar peaks.

3.3. Analysis of the Total Magnetic Field (TMF)

The corrected and georeferenced TMF maps revealed multiple localised anomalies of varying intensity, with amplitudes ranging from 2 to 18 nT. At 2 m, the anomalies displayed clear dipolar signatures typical of shallow ferromagnetic objects, whereas the 7 m anomalies appeared attenuated, exhibiting a 40–60% reduction in amplitude. Figure 11 compares the corrected TMF for the 2 m (a) and 7 m (b) flight heights.

 doi:10.20944/preprints202512.0511.v1

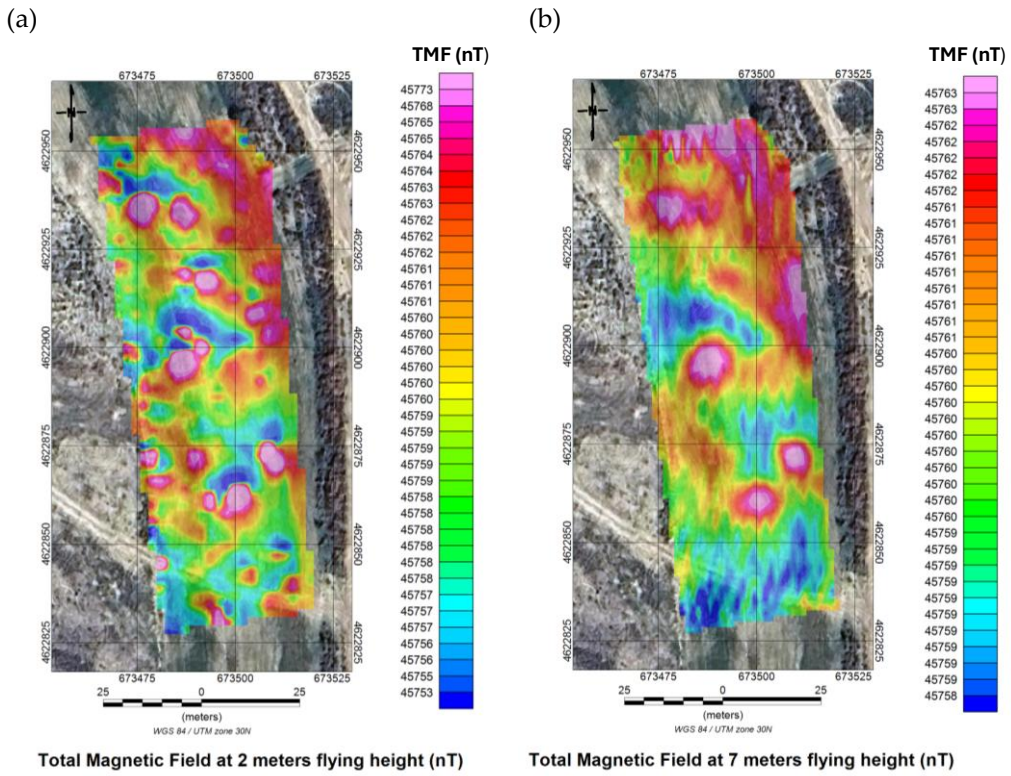

Figure 11. Comparison of the corrected total magnetic field for the 2 m flight (a) and the 7 m flight (b). WGS84/UTM zone 30N (scale in nT).

The spatial positions of these anomalies matched the known coordinates of the buried UXO surrogates, confirming the sensitivity of the system and validating a geolocation accuracy of approximately 0.5 m. All ferromagnetic metallic cylindrical objects were detected, while the plastic anti-tank control projectile produced no detectable magnetic response.

3.4. Reduction to the Pole (RTP)

Reduction to the pole (RTP) was applied to transform asymmetrical dipolar anomalies—produced by the local magnetic inclination of ~60°—into centered and more symmetrical responses [31]. This processing step facilitates interpretation by removing directional bias, improving anomaly localisation, and enhancing the distinction between UXO signatures and broader geological noise. RTP is especially useful at mid-latitudes, where dipolar skewing is significant. After RTP transformation, all UXO-related anomalies appeared as compact bodies with maxima centered over the true locations, allowing for a more accurate estimation of their lateral extent (e.g., diameters of 1–2 m for larger metallic cylindrical objects). The method reduced false positives by approximately 20%.

Figure 11 displays the RTP-transformed magnetic field for the 2 m (a) and 7 m (b) flights [28].

 doi:10.20944/preprints202512.0511.v1

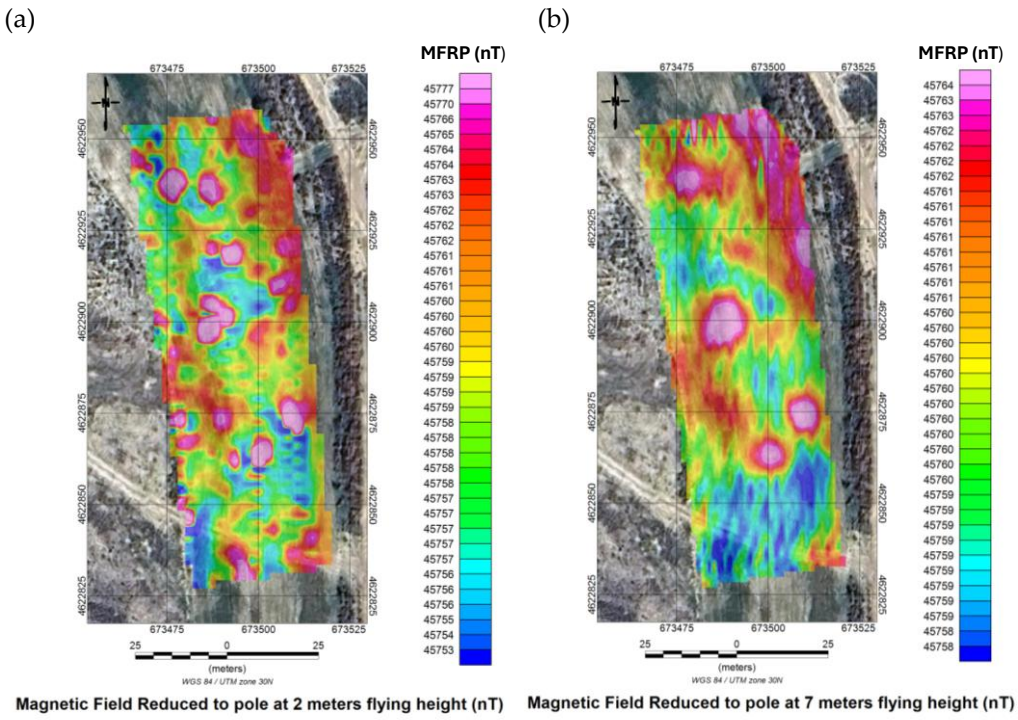

Figure 12. Total magnetic field reduced to the pole for the 2 m flight (a) and the 7 m flight (b). WGS84/UTM zone 30N (scale in nT).

3.5. Analytic Signal

Computation of the analytic signal enhanced magnetic gradients and sharply delineated the boundaries of magnetic sources. This technique effectively distinguished discrete anomalies compatible with buried UXO from diffuse signals associated with surface shrapnel or spent casings. Analytic-signal amplitudes exceeded 5 nT/m for UXO, whereas background ferromagnetic debris generally exhibited values <2 nT/m.

All eleven UXO surrogates produced clear, isolatable analytic-signal peaks, each reflecting its specific size, shape, and burial depth. Larger metallic cylindrical objects (120 and 155 mm) generated broad, high-amplitude responses (up to 15 nT/m), while smaller diameters (60 and 81 mm) showed attenuated but still distinct responses at 2 m altitude (3–5 nT/m) [29].

Figure 13 presents the analytic signal calculated for the 2 m (a) and 7 m (b) datasets.

Preprints.org (www.preprints.org) | NOT PEER-REVIEWED | Posted: 4 December 2025 doi:10.20944/preprints202512.0511.v1

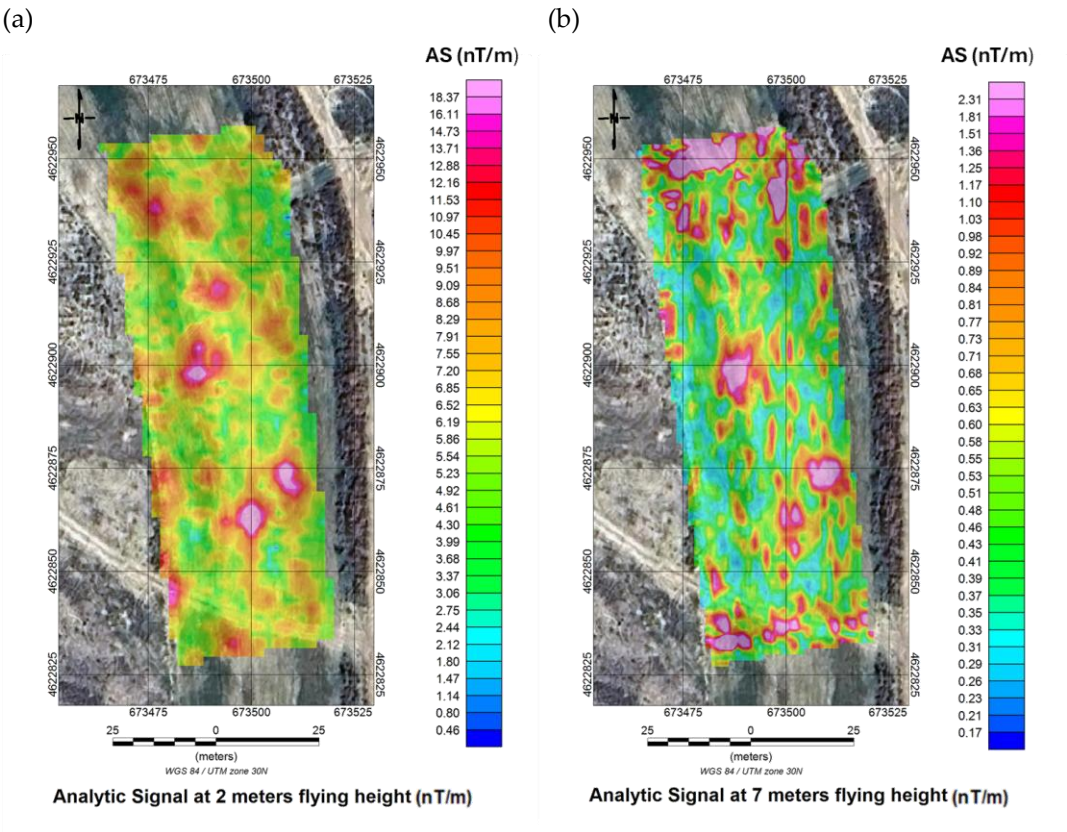

Figure 13. Analytic signal of the magnetic field calculated at 2 m (a) and 7 m (b) altitude. WGS84/UTM zone 30N (scale in nT/m).

Figure 14 shows a 3D view of the analytic signal for the 2 m flight draped over satellite imagery.

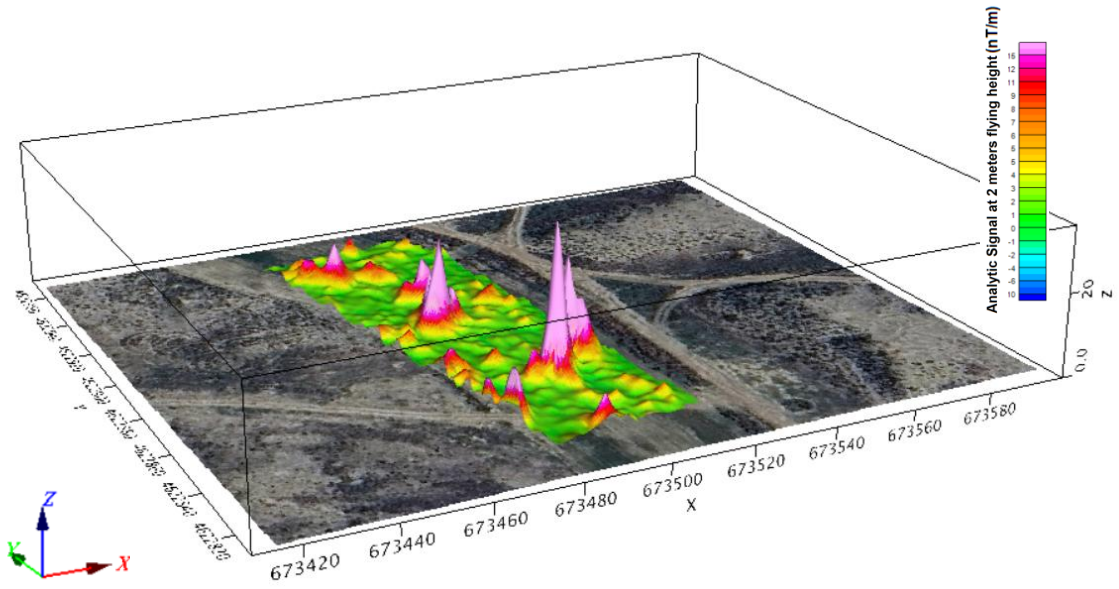

Figure 14. Three-dimensional view of the analytic signal (2 m flight) superimposed on satellite imagery. WGS84/UTM zone 30N (scale in nT/m).

3.6. Correlation Between Analytic Signal and UXO Positions

The analytic-signal maps obtained at 2 m (a) and 7 m (b) show a clear correlation with the known positions of the buried UXO surrogates.

 doi:10.20944/preprints202512.0511.v1

At 2 m height, a direct correspondence is evident between local analytic-signal maxima (up to 15 nT/m) and all ferromagnetic UXO, confirming a detection accuracy of approximately 0.5 m. As expected, the non-ferrous control projectile produced no detectable anomaly, reinforcing the selective sensitivity of the method to ferromagnetic materials. At 7 m height, the same anomalies remain visible but show attenuation (~50% reduction) and reduced definition, demonstrating the impact of increased height on anomaly resolution. Numerous additional low-intensity anomalies (2–5 nT/m) of irregular geometry were also detected; these are unrelated to the experimentally buried UXO and likely correspond to residual ferromagnetic debris commonly present in active large-scale outdoor ranges.

In summary, the analytic-signal maps confirm the technique's ability to detect and precisely locate ferromagnetic UXO, particularly at low height. However, the complex nature of active training ranges—with both controlled and uncontrolled metallic objects—requires careful interpretation and, ideally, prior knowledge of potential background sources. Figure 15 shows the analytic signal with UXO locations superimposed at 2 m (a) and 7 m (b).

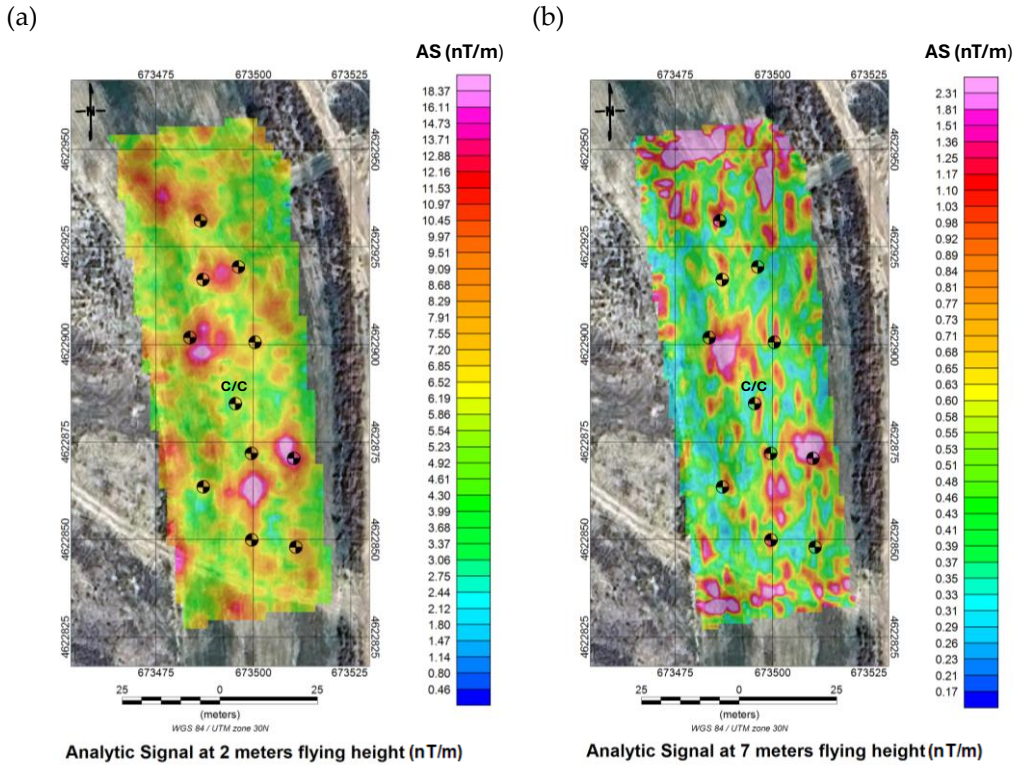

Figure 15. Analytic signal with superimposed UXO at 2 m (a) and 7 m (b) height. WGS84/UTM zone 30N (scale in nT/m).

To improve visualisation, thresholded representations of the analytic-signal maxima from the 2-m flight were generated using cut-off values of >6 nT/m and >7 nT/m. These approaches isolate significant anomalies and suppress background noise, allowing for rapid operational interpretation.

Figure 16 displays the thresholded analytic-signal maxima and their relationship to UXO positions.

 doi:10.20944/preprints202512.0511.v1

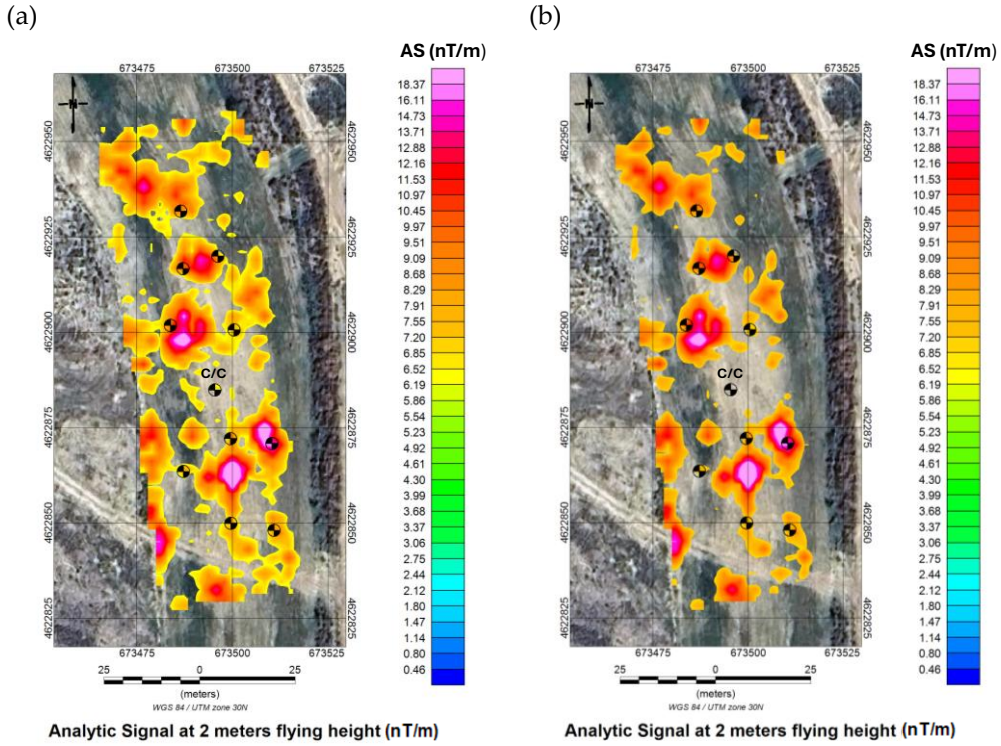

Figure 16. Thresholded areas of maximum analytic signal at 2 m height, >6 nT/m (a) and >7 nT/m (b), with the location of buried UXOs. WGS84/UTM zone 30N (scale in nT/m).

Figure 16 highlights that most ferromagnetic UXO fall within or immediately adjacent to the analytic-signal maxima, whereas the non-ferrous C/C UXO does not. Additional anomalies not associated with the buried UXO emphasise the complexity of detection in real military environments.

This threshold-based representation is operationally valuable because it enables prioritisation of ground inspection areas by filtering out diffuse magnetic noise and highlighting only high-intensity responses, thereby improving field efficiency.

The analytic-signal response was particularly effective in discriminating UXO-like anomalies from diffuse background clutter. Peak amplitudes of the analytic signal correlated directly with object size and burial depth, confirming the capability of this processing step to detect weak, short-wavelength signatures in noisy settings.

3.6. 3D Inversion Modelling

Three-dimensional magnetic susceptibility inversion [20, 21] was performed using Oasis Montaj Software to estimate the geometry and depth of the detected sources. In all cases, the estimated depth was <1 m, consistent with the true burial depths.

Figure 17a illustrates the discretisation mesh used for the 3D susceptibility inversion model. Figure 17b presents the resulting 3D susceptibility model, showing the distribution of magnetic contrasts in SI units.

 doi:10.20944/preprints202512.0511.v1

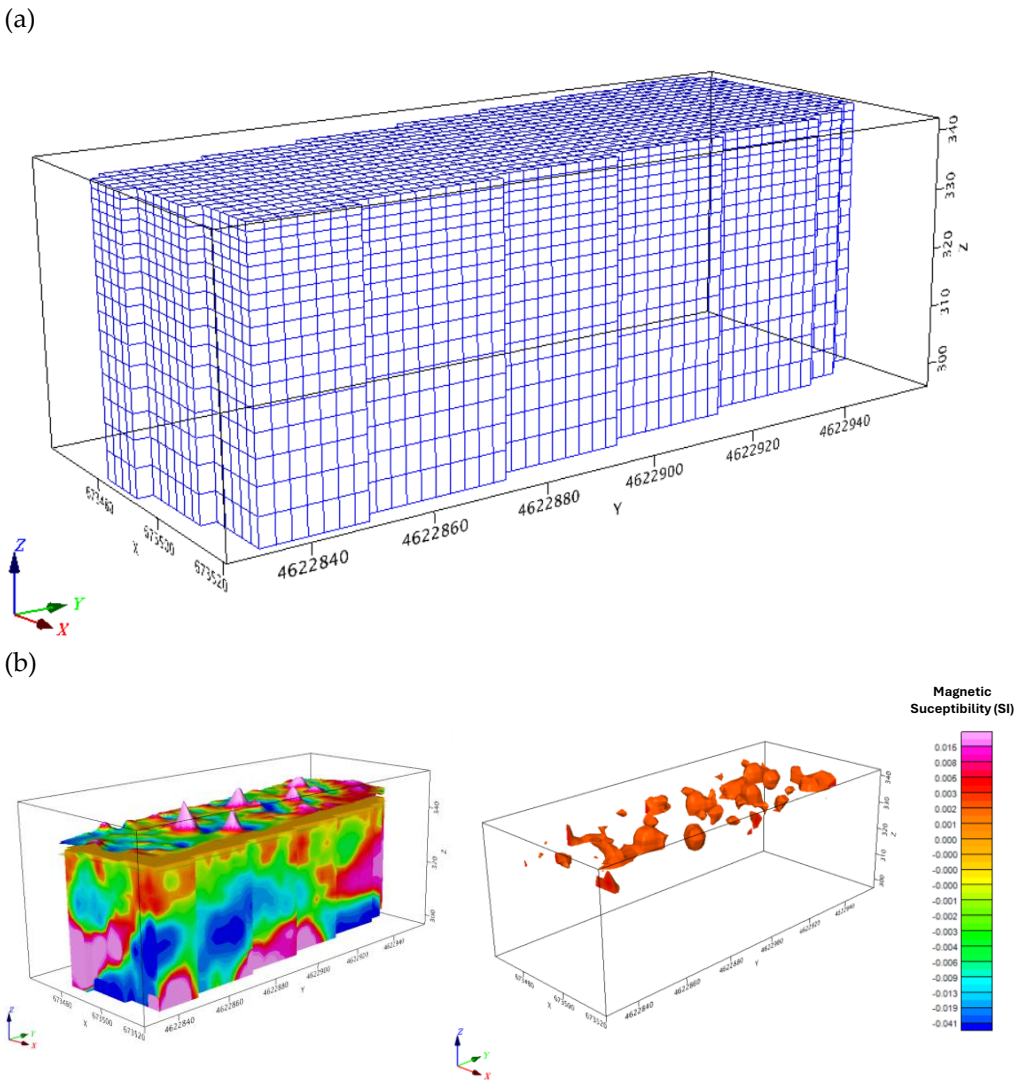

Figure 17. (a) Discretisation mesh used for the 3D magnetic susceptibility inversion model. WGS84/UTM zone 30N (scale in meters). (b) Results of the 3D magnetic susceptibility inversion model showing the three-dimensional distribution of anomalies. WGS84/UTM zone 30N (scale in SI units).

The left panel of Figure 17b displays the full 3D model, where high-susceptibility regions (>0.005 SI, shown in pink/red) appear near the surface and correspond to the UXO and other metallic debris. A complete 3D susceptibility volume extending to 40 m depth was also generated to distinguish near-surface anomalies from deeper geological structures. The right panel of Figure 17b shows a shallow cut of the model restricted to the upper portion of the inverted volume, where positive-susceptibility isosurfaces highlight the most relevant near-surface sources. This representation suppresses deeper geological background and focuses on discrete, compact bodies indicative of potential UXO, confirming the clustering of ferromagnetic sources near the surface and reinforcing the utility of low-altitude surveys for detection.

4. Discussion

A key outcome of this work is the demonstration that UAV-based magnetometry becomes operationally viable only when supported by a robust processing workflow. The spectral transformations and inversion techniques applied here were fundamental to enhancing anomaly detectability, mitigating the effects of intense ferromagnetic clutter, and improving localisation accuracy.

The results obtained in this study confirm that aerial drone-based aeromagnetic surveying is an effective tool for detecting UXOs under realistic operational conditions. The integrated analysis of

 doi:10.20944/preprints202512.0511.v1

total magnetic field maps and derived transformations (reduction to the pole, analytic signal, and 3D inversion) demonstrates that even small metallic objects can be reliably detected when flight heights remain below 3 m and high-sensitivity sensors are combined with dense acquisition grids.

4.1. Influence of Flight Altitude

The surveys conducted at 2 m and 7 m above ground level revealed a marked contrast in the amplitude and definition of the recorded anomalies. At 2 m, the magnetic responses of all metallic cylindrical objects were clearly identifiable, with signal-to-noise ratios exceeding 5. At 7 m, however, detection of smaller diameters (60 and 81 mm) was significantly weaker and, in some cases, approached the ambient magnetic noise threshold.

These findings are consistent with previous studies [6, 11] that emphasise the cubic attenuation of magnetic anomalies with sensor–target distance and reinforce the need to operate at low heights to reliably detect small or deeper-buried objects. Nevertheless, low-height operations impose higher demands in terms of flight precision, safety, and the need for accurate DTMs. Similar observations have been reported in controlled experimental sites, but the present study validates them in a heavily contaminated active controlled outdoor testing/training area.

4.2. Complexity of the Ferromagnetic Environment

San Gregorio Training Center represents a particularly challenging environment due to its high density of scattered metallic debris (shrapnel, casings, and surface scrap), which generates substantial background noise capable of masking weaker anomalies if not properly filtered. Under these conditions, diurnal correction, reduction to the pole and analytic-signal processing proved essential for discriminating between localised anomalies attributable to UXO and diffuse signatures caused by superficial debris.

Despite this complexity, the system successfully located all eleven buried UXO at known positions, demonstrating the robustness of the methodology and its selectivity in distinguishing ferromagnetic objects from non-ferrous materials, as shown by the negative control projectile.

4.3. Efficiency Compared with Ground-Based Methods

Ground-based magnetometry using handheld or towed sensors generally provides high proximity to the target and excellent local resolution, but acquisition times are longer and operators must physically enter potentially hazardous areas. In contrast, aerial drone-based surveys allow rapid coverage of large areas with minimal personnel exposure

In this study, the entire 0.53 ha grid was surveyed in under one hour of effective flight time, achieving a sampling density of one measurement every 25 cm (derived from 1 m line spacing and a 20 Hz sampling rate at 5 m/s). This resolution is comparable to or higher than many terrestrial methods, while maintaining a geolocation accuracy of approximately 0.5 m due to precise DTM integration and post-processing corrections. These results support the growing consensus that aerial drone magnetometry can complement or partially replace ground-based methods in UXO risk assessments.

4.4. Reliability of 3D Modelling

Three-dimensional magnetic susceptibility inversion [20, 21] provided accurate estimates of the geometry and depth of buried objects, confirming its value for delineating priority areas. However, model reliability decreases when anomalies are closely spaced or when flight height increases, conditions that reduce vertical and lateral resolution. In such cases, overlapping magnetic responses may complicate conventional inversion.

Future enhancements may include joint inversion algorithms, hybrid approaches integrating GPR or Light Detection and Ranging (LiDAR)-derived terrain models, and machine-learning tools

 doi:10.20944/preprints202512.0511.v1

capable of resolving complex multi-body interactions to improve 3D interpretation in cluttered environments.

4.5. Implications for CENAD Management

The successful validation of this methodology provides a promising pathway for optimising reconnaissance and hazard mitigation tasks in controlled outdoor testing/training areas. Integrating routine aerial drone magnetometry into post-exercise inspection procedures could substantially reduce accident risks and improve the management of UXO-contaminated zones by decreasing both the time and cost associated with manual clearance. Moreover, the generation of objective, georeferenced datasets enables the prioritisation of critical areas and supports targeted terrestrial interventions, enhancing personnel safety and operational efficiency. The achieved geolocation accuracy (~0.5 m) is sufficient to direct specialised teams toward precise locations with high confidence, reducing manual search time and improving resource allocation. These findings highlight the potential for aerial drone-based magnetic surveys to become an integral component of UXO risk mitigation strategies in active training facilities, aligning with broader efforts to modernise military environmental management practices. Future research may explore operational integration at larger scales, real-time processing capabilities, and multi-sensor fusion to further improve detection reliability.

5. Conclusions

This study demonstrates the technical and operational feasibility of drone-based aeromagnetic surveying as an effective tool for detecting UXOs in controlled outdoor testing/training areas characterised by real and substantial environmental complexity. The combination of high-sensitivity sensors, low-altitude flights, and advanced processing techniques enabled the accurate detection and localisation of the eleven metallic cylindrical objects intentionally buried in the study area of the CENAD.

The results underscore the importance of rigorous flight planning, including the use of a high-accuracy DTM to maintain constant height, as well as the application of diurnal corrections and spectral transformations to optimise detection performance.

This research contributes several novel and differentiated insights to the state of the art in airborne magnetometric UXO detection. The work was conducted in controlled experimental conditions within CENAD San Gregorio—the largest controlled outdoor testing/training area in Europe (33,000 ha) with more than 70 years of continuous activity—providing the first documented validation of aerial drone magnetometry in an actively used European training range. The site exhibits extreme ferromagnetic contamination, with background noise levels exceeding 10 nT RMS, far more challenging than the controlled environments commonly employed in previous studies and representative of real operational conditions involving thousands of metallic fragments, strong spatial variability of magnetic noise, and genuine difficulties in differentiating relevant signals from background clutter.

Two consecutive surveys were conducted at distinct operational heights (2 m and 7 m) over the same set of buried targets, enabling a direct and rigorous quantification of the trade-off between spatial resolution—favoured at low altitude—and operational feasibility—improved at higher altitude. Such a systematic comparison is largely absent from prior literature and provides essential data for establishing flight-protocol recommendations according to specific detection objectives.

Quantitative validation relied on full geodetic ground truth: eleven UXOs of varying diameters (60, 81, 105, 120, and 155 mm) were buried at controlled depths (20–60 cm) and surveyed using differential GNSS with sub-5-cm precision. A non-ferrous anti-tank projectile served as a negative control, enabling objective performance metrics to be calculated, including detection rates by caliber and depth, RMS geolocation accuracy, material-specific discrimination capability, altitude-dependent signal-to-noise ratios, and operational detectability thresholds in cluttered environments.

 doi:10.20944/preprints202512.0511.v1

The study proposes a fully replicable, integrated methodological workflow spanning: high-accuracy DTM generation, flight-path design with constant altitude maintenance, autonomy calculations, sensor configuration, establishment of base stations for diurnal correction, data acquisition, precise georeferencing, noise filtering, spectral transformations (reduction to the pole, analytic signal), 3D magnetic susceptibility inversion, and final UXO interpretation, discrimination, and prioritization of areas for ground inspection.

Concrete operational metrics achieved under real field conditions include:

– coverage of 0.53 ha in <1 hour of effective flight,

– sampling density of ~50,000 points/ha (25 cm point spacing),

– anomaly geolocation accuracy of 0.5 m RMSE,

– 100% detectability of ferromagnetic UXOs ≥60 mm buried <60 cm at 2 m flight height,

– signal-to-noise ratios >5 for all ferromagnetic UXOs under low-altitude conditions.

The study also confirms operational feasibility under geomagnetic conditions typical of mid-latitudes in Europe (inclination ~60°), validating that spectral transformations such as reduction to the pole—originally developed for mineral exploration—are effective for enhancing UXO-related magnetic anomalies under these geomagnetic parameters [28, 30].

Importantly, by conducting experiments under deliberately non-ideal conditions, including scattered vegetation, irregular microtopography, and severe ferromagnetic contamination, the study documents the practical limitations of the method: vegetation effects on flight accuracy and DTM quality, increased false-positive rates due to metallic clutter, post-processing requirements for reliable discrimination, reduced detectability at altitudes above 7 m, and interpretation challenges in the presence of multiple overlapping anomalies. These insights are essential for informed decision-making regarding operational implementation and establish benchmark criteria for evaluating similar systems and assessing cost-benefit trade-offs relative to alternative technologies.

Key findings include:

-High sensitivity and spatial resolution.

-Low-altitude flights (2 m AGL) combined with a dense acquisition grid (1 m spacing) enabled reliable detection of UXO of all diameters, including 60 mm, with signal-to-noise ratios >5.

-Robustness against ferromagnetic clutter.

-Diurnal magnetic-field correction, combined with spectral transformations (RTP, analytic signal) and 3D inversion, improved the separation of UXO-related anomalies from the diffuse responses generated by metallic debris, enhancing discrimination by roughly ~20%.

-Operational reliability and safety.

-Aerial drones surveys reduced acquisition time (<1 h for 0.53 ha) and eliminated the need for personnel to enter hazardous areas, increasing safety while producing systematic, repeatable coverage suitable for long-term monitoring.

-Geolocation precision.

-Integration of DTM-based altitude control, diurnal corrections, and advanced processing provided geolocation accuracy of ~0.5 m, enabling targeted terrestrial follow-up operations.

-Strategic utility.

-The methodology can be integrated into post-exercise verification protocols and UXO-contamination assessments, thereby improving management and remediation of controlled outdoor testing/training areas.

Overall, drone-based aeromagnetic surveying emerges as a practical, precise, and scalable solution to one of the key challenges in the safety and management of military training ranges: the rapid and safe detection of UXOs located outside designated designated landing areas. Rather than replacing terrestrial methods, this technology provides an efficient pre-classification and prioritisation tool that enhances the effectiveness of subsequent ground operations.

This study focused on a specific environment and controlled burial conditions. Future research should validate the methodology under varying burial depths, UXO densities, and soil magnetic properties. Comparisons with alternative airborne systems (e.g., multi-sensor arrays, hyperspectral

 doi:10.20944/preprints202512.0511.v1

payloads) and applications in training areas with different geomagnetic characteristics would also be valuable.

The study highlights the decisive role of the magnetic data–processing workflow. The combination of diurnal correction, filtering, RTP, analytic-signal computation, and 3-D inversion constitutes a reproducible technical sequence that substantially increases the detectability of weak magnetic anomalies in complex environments.

Future research directions should include integrating airborne magnetometry with complementary technologies such as ground-penetrating radar (GPR), LiDAR, and hyperspectral sensors to improve multiparametric UXO characterisation, as well as implementing machine-learning algorithms for automated anomaly classification and intelligent discrimination between targets of interest and ferromagnetic clutter. Comparative campaigns across Spanish and European training ranges—under varying geological, geomagnetic, and topographic conditions—are essential for developing standardized operational procedures that support routine integration of this technology into post-exercise inspection protocols at CENAD and other active controlled outdoor testing/training areas.

Author Contributions: The first author (I.U-G.) is currently conducting his doctoral research on the application of geotechnologies in controlled outdoor testing/training areas and led the overall development of the study. Conceptualization, I.U-G. and D.G-A.; methodology, I.U-G.; software, I.U-G. P.C-G, J. C-G; validation, I.U-G., D.G-A., D.G-S, and P.C-G.; formal analysis, I.U-G.; investigation, I.U-G.; resources, D.G-A; data curation, I.U-G.; writing—original draft preparation, I.U-G.; writing—review and editing, D.G.-A; visualization, I.U.-G; supervision, D.G.-A; project administration, D.G.-A; funding acquisition, D.G.-A. The corresponding author (D.G-A.) is the doctoral supervisor and head of the TIDOP research group, contributing expertise in geotechnologies and overseeing the scientific development of the work. The third and fourth authors (P.C-G., J.C-G.) are specialist in magnetometry, including airborne systems, and contributed technical expertise to the design, interpretation, and validation of the magnetic measurements. The second author (D.G-S.) is an expert in UAV systems and contributed specialised knowledge on drone integration, flight planning, and operational management. All authors have read and agreed to the published version of the manuscript.

Funding: This research received no external funding.

Data Availability Statement: The data supporting the findings of this study are available from the corresponding author upon reasonable request. Due to the sensitive nature of the controlled outdoor testing/training area where the experiment was conducted, the complete dataset cannot be publicly released. No publicly archived datasets were generated or analysed during the study.

DURC Statement: The present research is restricted to the defense and civilian application of aerial drone magnetometry for the detection of unexploded ordnance (UXO). One of the principal beneficial outcomes of this study is its contribution to humanitarian demining, as the proposed methodology enables the remote detection of buried landmines and UXO without exposing human personnel to danger. By allowing survey operations to be carried out from the air, this approach significantly reduces the risk to demining teams and supports safer, more efficient clearance activities in contaminated areas. The study does not involve the development, testing, or enhancement of weapon systems, nor does it pose any foreseeable risk to public health, safety, or national security. The authors acknowledge the potential dual-use nature of geophysical sensing technologies and confirm that all activities were conducted in full compliance with applicable national and international regulations governing dual-use research. In line with ethical responsibilities, the authors have implemented appropriate safeguards, adhered to responsible research practices, and ensured transparent reporting to minimise any risk of misuse. The research is therefore directed solely towards beneficial, peaceful, and humanitarian applications, contributing to safer environments in post-conflict regions.

Acknowledgments: The authors thank the personnel of the San Gregorio Training Center (CENAD) for their logistical support during the field campaign. The authors also acknowledge the technical assistance provided by the TIDOP Research Group (University of Salamanca) in the aerial drone integration and geophysical data

 doi:10.20944/preprints202512.0511.v1

processing. The authors would like to acknowledge Seequent for their support and the useof Oasis Montaj software, which was essential for the development of this work.

Conflicts of Interest: The authors declare no conflicts of interest. The funders had no role in the design of the study; in the collection, analyses, or interpretation of data; in the writing of the manuscript; or in the decision to publish the results.

References

1. Porsani, J.L.; Sauck, W.A.; Sobrinho, J.A.; Barreto, M.S. UXO Detection from Aeromagnetic and Ground Penetrating Radar Data at a 20th Century Battlefield. J. *Appl. Geophys*. **2004**, 56, 155–169. https://doi.org/10.1016/j.jappgeo.2004.08.003
2. Sanderson, N.; Reid, P. Magnetic Properties of Military Scrap Metal. Geophys. *Prospect*. **2010**, 58, 1033–1044. https://doi.org/10.1111/j.1365-2478.2010.00891.x
3. Sattel, D. Modelling of Magnetic Clutter in UXO Sites. J. *Appl. Geophys*. **2010**, 70, 195–203. https://doi.org/10.1016/j.jappgeo.2009.12.001
4. Walter, C.A.; Braun, A.; Fotopoulos, G. Impact of Three-Dimensional Attitude Variations of an Unmanned Aerial Vehicle Magnetometry System on Magnetic Data Quality. *Geophys. Prospect*. **2019**, 67, 465–479. https://doi.org/10.1111/1365-2478.12732
5. Mu, Y.; Xie, W.; Zhang, X.; Zheng, Y. The Joint UAV-Borne Magnetic Detection System and Cart-Mounted Time Domain Electromagnetic System for UXO Detection. *Remote Sens*. **2020**, 12, 2343. https://doi.org/10.3390/rs12152343.
6. Park, J.S.; Choi, J.H.; Kim, B.Y.; Lee, M.J.; Jo, H.W. Application of a Drone Magnetometer System to Military Mine Detection in the Demilitarized Zone. *Sensors*. **2021**, 21, 3175. https://doi.org/10.3390/s21093175
7. Billings, S.; Walker, S. Magnetic Signatures of Unexploded Ordnance: A Complete Review. *Sensors*. **2017**, 17, 2540. https://doi.org/10.3390/s17112540
8. Zhdanov, M.S. Geophysical Electromagnetic Theory and Methods; Elsevier: Amsterdam, The Netherlands, 2009. https://doi.org/10.1016/B978-0-12-396538-9.00001-1.
9. Leliak, P.; Schmidt, W.; Barrow, B. Integrated GPR–Magnetometry for Detection of Shallow UXO. *Environ. Eng. Geophys*. **2017**, 22, 219–231. https://doi.org/10.2113/JEEG22.2.219.
10. Zhdanov, M.S. Inverse Theory and Electromagnetic Applications; Elsevier: Amsterdam, The Netherlands, 2015. https://doi.org/10.1016/C2013-0-19143-1
11. Nabighian, M.N.; Ander, M.E.; Grauch, V.J.S.; Hansen, R.O.; LaFehr, T.R.; Li, Y.; Pearson, W.C.; Peirce, J.W.; Phillips, J.D.; Ruder, M.E. The Historical Development of the Magnetic Method in Exploration. *Geophysics*. **2005**, 70, 33ND–61ND. https://doi.org/10.1190/1.2133784.
12. Pašteka, R. Interpretation of Magnetic Dipoles in Cluttered Environments. *Appl. Geophys*. **2017**, 145, 54–67. https://doi.org/10.1016/j.jappgeo.2017.07.002
13. Chen, R.; Guo, Y.; Li, X. Compensation of Magnetic Interference for UAV-Mounted Magnetometers. *Meas. Sci. Technol*. **2018**, 29, 065902. https://doi.org/10.1088/1361-6501/aabf0c.
14. Martin, R.; Chadebec, O.; Roussel, J.; Riu, D. Impact of UAV Attitude and Aerodynamic Forces on Airborne Magnetometer Data. *IEEE Trans. Geosci. Remote Sens*. **2021**, 59, 7420–7432. https://doi.org/10.1109/TGRS.2020.3028740
15. Brants, M.; Kucenko, S. UAV-Based Magnetometer Comparison: UXO Test. SPH Engineering & sUAS News 2023.
16. Smith, R.; Billings, S.; Pasion, L. Evaluation of Airborne Magnetometry for UXO Detection. *Environ. Eng. Geophys.* **2018**, 23, 45–59. https://doi.org/10.2113/JEEG23.1.45.
17. Zakharov, V.; Samsonov, S.; Tiampo, K.; Smirnov, M. Low-Altitude UAV Aeromagnetic Surveys in High-Noise Environments. *Sensors*. **2020**, 20, 4335. https://doi.org/10.3390/s20154335.
18. Jordan, C.; Heaney, M.; Marsh, R.; Green, M. Development of UAV Magnetometry for UXO Detection in Coastal Environments. *Remote Sens.* **2022**, 14, 1211. https://doi.org/10.3390/rs14051211.
19. Li, Y.; Oldenburg, D.W. 3-D Inversion of Magnetic Data. *Geophysics*. **1996**, 61, 394–408. https://doi.org/10.1190/1.1443968.

20. Sun, J.; Li, Y. Adaptive Regularization for Magnetic Data Inversion. *Geophysics*. **2015**, 80, J1–J12. https://doi.org/10.1190/geo2014-0191.1.
21. Pasion, L.; Oldenburg, D. Locating UXO Using the Magnetic Gradient Tensor. *Geophysics*. **2001**, 66, 571–582. https://doi.org/10.1190/1.1444943.
22. Chen, C.; Huang, Y. Discrimination of UXO Using Magnetic Amplitude Data. *IEEE Trans. Geosci. Remote Sens.* **2020**. https://doi.org/10.1109/TGRS.2020.2970645.
23. Farquharson, C.; Oldenburg, D.W. A Comparison of Automatic Techniques for Estimating Magnetization Direction. *Geophysics*. **1998**, 63, 194–204. https://doi.org/10.1190/1.1444322.
24. Hansen, R.; Pawlowski, R. Analytic Signal Methods for High-Noise Magnetic Environments. *Geophysics*. **2005**, 70, L63–L65. https://doi.org/10.1190/1.1988180.
25. Parshin, A.; Abramov, S.; et al. UAV-Based Magnetometry System for Detection of Ferromagnetic Objects. *Sensors*. **2022**, 22, 8341. https://doi.org/10.3390/s22218341
26. Oldenburg, D.W.; Li, Y. Depth Estimation and Inversion of Magnetic Data. *Geophysics*. **1999**, 64, 123–135. https://doi.org/10.1190/1.1444513.
27. Malehmir, A.; Dynesius, L.; Paulusson, K.; Paulusson, A.; Johansson, H.; Bastani, M.; Wedmark, M.; Lindgren, S. UAV-Based Magnetometry for Mineral Exploration: A Case Study. *Geophysics*. **2017**, 82, B47–B61. https://doi.org/10.1190/geo2016-0351.1.
28. Chen, C.; Zhou, Q.; Li, X. Advanced Analytic Signal Processing for Magnetic Interpretation. *Appl. Geophys.* **2020**, 180, 104135. https://doi.org/10.1016/j.jappgeo.2020.104135
29. Zhdanov, M.S. Numerical Methods in Electromagnetic Inversion. *Surv. Geophys.* **2011**, 32, 1–40. https://doi.org/10.1007/s10712-010-9094-z.
30. Pašteka, R.; Richter, C.; Starek, M. Magnetic Inversion in Noisy Environments. *Appl. Geophys.* **2015**, 119, 114–127. https://doi.org/10.1016/j.jappgeo.2015.05.011.
31. Cooper, G.R.J.; Cowan, D.R. The Application of RTP at Low Magnetic Latitudes. *Geophysics*, **2006**, 71, L77–L82. https://doi.org/10.1190/1.2338338.